

Antiferromagnetic resonances in twinned EuFe_2As_2 single crystals

I. A. Golovchanskiy ^{1,2,3,4,*}, N. N. Abramov ², V. A. Vlasenko,⁵ K. Pervakov,⁵ I. V. Shchetinin ², P. S. Dzhumayev,^{2,4}
 O. V. Emelyanova,^{2,4,6} D. S. Baranov ^{1,3,4,7}, D. S. Kalashnikov,^{1,3} K. B. Polevoy ^{1,3}
 V. M. Pudalov ^{5,8} and V. S. Stolyarov^{1,2,3}

¹Center for Advanced Mesoscience and Nanotechnology, Moscow Institute of Physics and Technology, National Research University,
 9 Institutskiy Pereulok, Dolgoprudny, Moscow Region 141700, Russia

²National University of Science and Technology MISIS, 4 Leninsky Prospekt, Moscow 119049, Russia

³Dukhov Research Institute of Automatics (VNIIA), Moscow 127055, Russia

⁴National Research Nuclear University MEPhI (Moscow Engineering Physics Institute), 31 Kashirskoye Shosse, Moscow 115409, Russia

⁵Ginzburg Center for High Temperature Superconductivity and Quantum Materials, P.N. Lebedev Physical Institute of the RAS,
 Moscow 119991, Russia

⁶Center for Energy Science and Technology, Skolkovo Institute of Science and Technology, Nobel Street 3, Moscow 121205, Russia

⁷Skobeltsyn Institute of Nuclear Physics, MSU, Moscow 119991, Russia

⁸HSE University, Moscow 101000, Russia



(Received 10 December 2021; revised 13 April 2022; accepted 28 June 2022; published 14 July 2022)

In this paper, we report the results of magnetic resonance spectroscopy of EuFe_2As_2 single crystals. We observe magnetic resonance responses, which are attributed to antiferromagnetic resonances of the Eu sublattice with orthorhombic crystal structure and with different orientations of twin domains relative to the external field. We confirm the validity of the recently proposed spin Hamiltonian with anisotropic Eu-Eu exchange interaction and biquadratic Eu-Fe exchange interaction.

DOI: [10.1103/PhysRevB.106.024412](https://doi.org/10.1103/PhysRevB.106.024412)

I. INTRODUCTION

The discovery of the iron pnictide high-temperature superconductors has been one of the most striking discoveries in recent years in condensed-matter physics. In this class of materials, intriguing properties were recently found in the subclass of compounds originating from the parent EuFe_2As_2 [1–8]. Superconductivity in a EuFe_2As_2 -based ferromagnetic superconductor emerges by doping it with phosphorus [9–14], by substituting europium layers with rubidium [15–21], or by applying pressure [22,23]. In these materials the Fe $3d$ orbitals exhibit a dual itinerant-localized magnetism and, simultaneously, participate in superconducting pairing. When it comes to the interplay between the superconductivity and the ferromagnetism, the studies are mainly focused on their superconducting properties and on the physical origin behind the emergence of superconductivity. In the case of EuFeAs -based ferromagnetic superconductors the coexistence is considered between magnetic ordering of Eu^{2+} ions with large spin number $S = 7/2$ and superconducting ordering of Fe- $3d$ electrons.

The EuFe_2As_2 compound itself is rich in various magnetic phenomena. Its magnetic structure was studied extensively in recent years using neutron scattering [4–6], x-ray scattering [24], nuclear magnetic resonance (NMR) [25], x-ray magnetic circular dichroism (XMCD) [8], and transport measurements [6]. At about 190 K the crystal structure of EuFe_2As_2 undergoes the tetragonal-to-orthorhombic phase transition [4,7,8] accompanied by the spin density wave antiferromagnetic transition in the Fe sublattice. The direction of spins in the spin

density wave is locked along the longer a crystal axis of the orthorhombic structure (see Fig. 1). At about 20 K the Eu subsystem undergoes the A-type antiferromagnetic transition [5,7,8]. The orthorhombic crystal structure is naturally subjected to twinning, while the Eu-Fe exchange interaction and large magnetoelastic coupling drive the detwinning of the crystal lattice. A possible scenario of the detwinning process in in-plane magnetic fields can be described as follows [5–7,25]. At zero field the crystal is twinned, and the structural domains with mutually perpendicular a axis are equally distributed in the sample. By applying an external field, domains having the a axis perpendicular to the external field (B domains) become energetically favored and grow. In these domains the Eu spins begin to deviate from the a axis to the direction of the external field, while the spins in opposite domains having the a axis along the external field (A domains) are robust and their directions are still maintained. In Refs. [6,7,25] it was discussed that this process continues until the B domains occupy the entire sample, while A domains vanish. With a further increasing magnetic field, the Eu spins in B domains keep deviating from their original direction, while the Eu spins in A domains flip along the external field direction. When the field exceeds the saturation field, all Eu spins are aligned with the external field, and A and B domains merge into a single A domain. In Ref. [6] it was reported that the structure of EuFe_2As_2 being field detwinned may persist at zero field.

This detwinning scenario, however, is under debate due to unclear role of the domain pinning. In fact, different groups report different magnetization curves of free unstressed EuFe_2As_2 single crystals (compare the magnetization

*Corresponding author: golov4anskiy@gmail.com

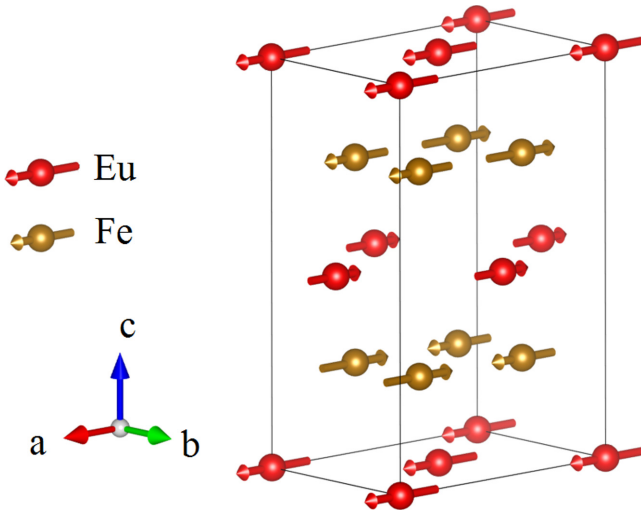


FIG. 1. Magnetic crystal structure of EuFe_2As_2 [made using Visualization for Electronic and Structural Analysis (VESTA) software]. The crystal structure of EuFe_2As_2 is orthorhombic with the space group $Fmmm$ [4]. The Fe spin sublattice is in the spin density wave antiferromagnetic state aligned with the a axis. The Eu spin sublattice is in the A-type antiferromagnetic state.

curves in Refs. [6,7] and in Refs. [3,26]), which indicates the dependence of sample properties on sample growth specifics. Notably, magnetization curves of free unstressed EuFe_2As_2 single crystals in Refs. [3,26] are consistent with magnetization curves of twinned EuFe_2As_2 single crystals with fixed population of domains [8], which is an indication of rather rigid domain pinning in some of EuFe_2As_2 single crystals.

Possible detwinning is one of the main obstacles for studies of magnetic ordering in EuFe_2As_2 with magnetization measurements: Upon magnetization the variation in populations of differently oriented twin domains additionally impacts the magnetization. Only recently has the complete microscopic form of magnetic interactions in EuFe_2As_2 been established [7,8]. It includes the anisotropic Eu-Eu exchange interaction and the biquadratic Eu-Fe exchange interaction and implies the spin-flip transition in the A-type antiferromagnetic Eu sublattice when the magnetic field is applied along the a crystal axis. Metamagnetic transitions in EuFe_2As_2 [3,8,26] are developed due to magnetization of twin domains with a $\pi/2$ difference in their orthorhombic orientation.

In this paper, we consider magnetization dynamics in single-crystal EuFe_2As_2 . In general, magnetic resonance (MR) measurements are the ultimate tool for testing anisotropy and interlayer exchange interactions in various antiferromagnets [27–32]. In addition, MR studies are free from the twinning problem, since the ratio of differently oriented twin domains impacts the intensity but not the position of resonance lines. By observing and analyzing MR spectral lines we have found that the MR spectrum confirms the validity of the three-dimensional (3D) expanded version of the spin Hamiltonian proposed in Ref. [8].

II. EXPERIMENTAL DETAILS

EuFe_2As_2 single crystals were grown using the self-flux method, by analogy with previous works [33,34].

The initial high-purity components of phase-homogeneous EuAs (99.95% Eu + 99.9999% As) obtained by the high-pressure technique and preliminary synthesized precursor Fe_2As (99.98% Fe + 99.9999% As) were mixed with a 1 : 6 molar ratio. The mixture in an alumina crucible was sealed in a niobium tube under residual argon pressure. The sealed container was loaded into a tube furnace with an argon atmosphere to prevent niobium oxidation. Then, the furnace was heated up to 1250 °C, held at this temperature for 24 h to homogenize melting, cooled down to 900 °C at a rate of 2 °C/h, and then cooled down to room temperature inside the furnace. Finally, crystals were collected from the crucible in an argon glovebox. Visually, as-grown bulk crystals demonstrate a well-defined layered structure and their pliability for cleavage and exfoliation along the layering direction only. X-ray diffraction (XRD) studies confirm the alignment of ab crystal planes within the layers and orientation of the c crystal axis across the layers. Magnetization measurements [35] show a steplike magnetization behavior consistent with Refs. [3,8,26]. Samples for magnetic resonance spectroscopy were obtained by cleavage of as-synthesized bulk crystals. Cleaved EuFe_2As_2 samples were a few millimeters in size along the ab crystal planes and about 50 μm thick along the c crystal axis, which ensured the “thin film” geometry with defined crystal orientation.

Magnetic resonance spectroscopy was performed using the vector-network-analyzer–magnetic-resonance (VNA-MR) flip-chip approach [36,37]. A cleaved EuFe_2As_2 sample is glued on top of the transmission line of the coplanar waveguide. The waveguide with impedance 50 Ω and a transmission line of width 0.5 mm is patterned on an Arlon AD1000 copper board and is equipped with subminiature push-on (SMP) rf connectors. The board with the sample is installed in a brass sample holder. A thermometer and a heater are attached directly to the holder for precise temperature control. The holder is placed in a homemade superconducting solenoid inside a closed-cycle cryostat (Oxford Instruments Triton, base temperature 1.2 K). A magnetic field is applied in plane along the direction of the waveguide. The response of the experimental samples is studied by analyzing the transmitted microwave signal $S_{21}(f, H)$ with the VNA Rohde & Schwarz ZVB20. This setup allows us to perform spectroscopy in the temperature range from 2 K up to 30 K, in the field range up to 1 T, and in the frequency range up to 26.5 GHz.

III. RESULTS AND DISCUSSION

Figure 2 shows MR absorption spectra of a EuFe_2As_2 sample measured with a magnetic field applied in plane along the ab layers at $T = 5$ and 20 K. At 5 K [Fig. 2(a)] the spectrum contains three absorption features (encircled with red dashed lines): (i) a resonance line at $0 < \mu_0 H \lesssim 0.5$ T and $10 < f < 23$ GHz with a negative-slope linear field dependence, referred to as line I; (ii) a weaker resonance line at $\mu_0 H \gtrsim 0.7$ T and $18 < f < 22$ GHz, which also has approximately linear field dependence with a negative slope, referred to as line II; and (iii) an absorption “patch” at $0.55 \lesssim \mu_0 H \lesssim 0.7$ T and $f > 20$ GHz, referred to as absorption feature III. A spectral line with a negative field slope is commonly attributed to an antiferromagnetic resonance response. Cross sections $S_{21}(H)$

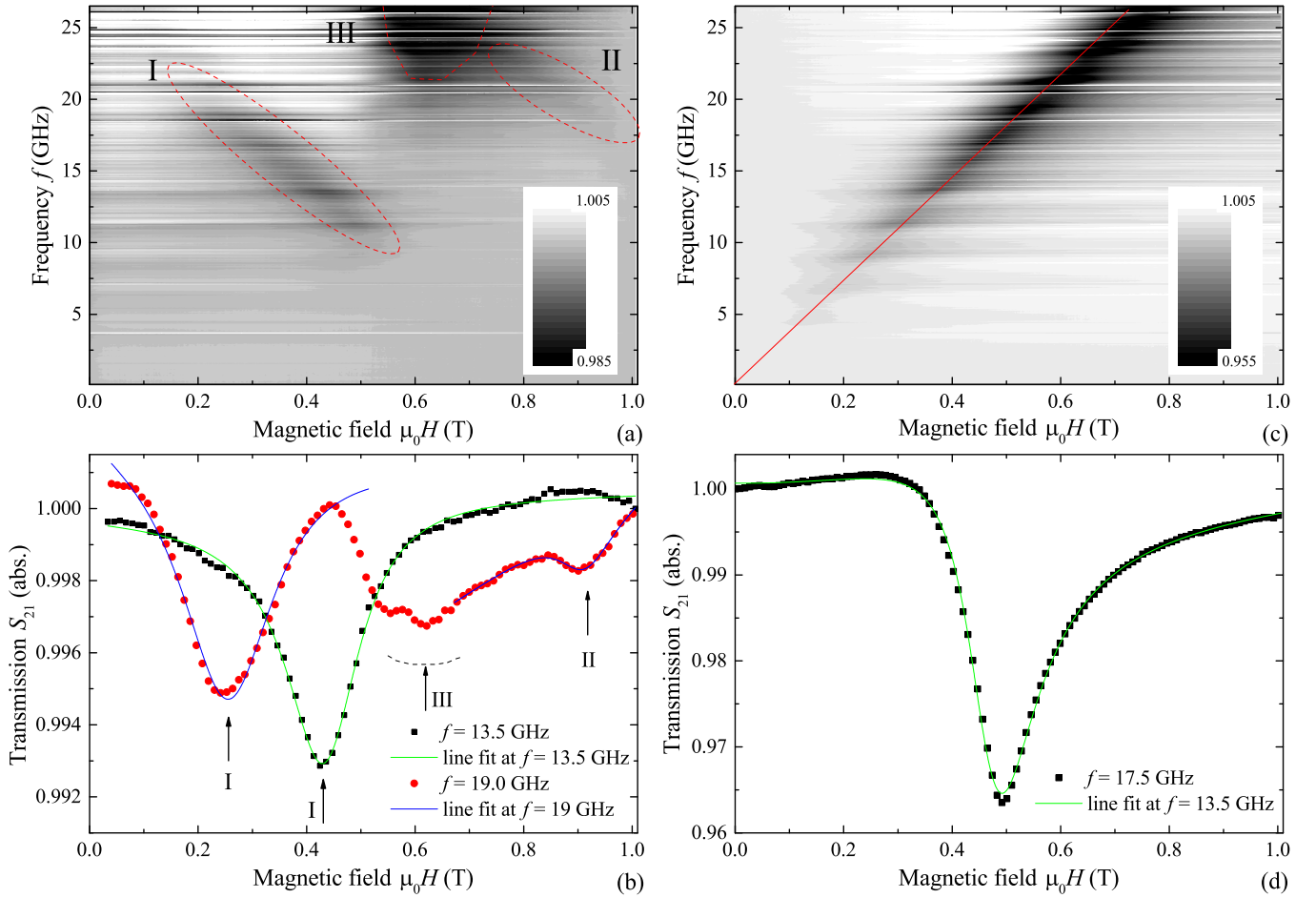


FIG. 2. (a) and (c) MR absorption spectra $S_{21}(f, H)$ of EuFe_2As_2 measured at $T = 5$ K (a) and 20 K (c). A magnetic field is applied in plane along the ab crystal planes. The red dashed lines in (a) highlight three absorption features. The red line in (c) corresponds to the linear fit of the spectral line with the slope 36.6 GHz/T. (b) and (d) Cross sections $S_{21}(H)$ of spectra at $T = 5$ K (b) and 20 K (d) at specified frequencies. Solid lines in (b) and (d) show the fit of resonance lines, while arrows indicate corresponding absorption features. Here, abs., denotes the absolute units, i.e., the ratio of the output signal to the input signal.

of the spectrum at 5 K and at selected frequencies are shown in Fig. 2(b). The $S_{21}(H)$ curves clearly indicate absorption peaks of resonance lines I and II. Derivation of the MR frequency dependence on the applied magnetic field $f_r(H)$ was performed by fitting $S_{21}(H)$ curves with the complex resonant susceptibility [37].

In contrast, at temperatures above 19 K the spectrum contains a single resonance line with approximately linear dependence of the resonance frequency on the magnetic field, corresponding to paramagnetic resonance of Eu spins. Figure 2(c) shows a representative example of the spectrum at $T = 20$ K. The field slope of the paramagnetic resonance at 20 K, $f_r/\mu_0H \approx 36.6$ GHz/T, is slightly higher than the gyromagnetic ratio of free electrons, 28 GHz/T. In addition, the resonance line shows some deviation from linear behavior. These effects are attributed to the residual susceptibility of the paramagnetic phase in the vicinity of the Curie temperature [38] and should be understood as follows. The magnetization of the paramagnetic phase is proportional to the applied field $M = \chi(T, H)H$. In the thin-film geometry the resonance frequency of the paramagnetic phase is still provided by the Kittel formula $2\pi f = \gamma\sqrt{H(H+M)} = \gamma H\sqrt{1 + \chi(T, H)}$.

At temperatures slightly above the Curie temperature, the magnetization $\chi(T, H)H$ is comparable to the saturation magnetization at high fields and shows a nonlinear dependence on H . These factors result in a larger slope of the linear fit and in some nonlinearity of the resonance line, which are observed in Fig. 2(c). At higher temperatures, $\chi(T, H)$ is gradually reduced, and the resonance line approaches the conventional paramagnetic one, which is observed at 25 and 30 K [35]. Figure 2(d) shows the cross section of the spectrum $S_{21}(H)$ at $f = 17.5$ GHz, which contains a single resonance peak, and its fit with the complex susceptibility.

The spin configuration of Eu and Fe subsystems in EuFe_2As_2 and the twinning problem were studied extensively in a number of previous works with neutron scattering and XMCD measurements. As a consensus view [8], it is shown that at low temperature the Fe sublattice is in the spin density wave antiferromagnetic state aligned with the longer side of orthorhombic lattice, while the Eu sublattice has the A-type antiferromagnetic order (see Fig. 1). Importantly, Eu-Fe exchange interaction results in anisotropic Eu-Eu exchange interaction and in the development of the easy axis along the direction of the spin density wave (a direction) due to

biquadratic Eu-Fe exchange. The total free energy of the spin configuration in a unit cell of Eu layers is [8]

$$F = 2(J + W)e_{1x}e_{2x} + 2(J - W)e_{1y}e_{2y} + 2Je_{1z}e_{2z} - 8K_a \sum_{i=1}^2 e_{ix}^2 + K_u \sum_{i=1}^2 e_{iz}^2 - M_s \sum_{i=1}^2 \vec{e}_i \vec{H}, \quad (1)$$

where (e_{ix}, e_{iy}, e_{iz}) is the unit vector of the ferromagnetic moment of the Eu atomic layer in spherical coordinates $\vec{e} = \sin \theta \cos \phi \hat{x} + \sin \theta \sin \phi \hat{y} + \cos \theta \hat{z}$, the $[\hat{x}, \hat{y}, \hat{z}]$ axes are aligned with the $[a, b, c]$ crystal axes in Fig. 1, respectively, the first three terms are the exchange interaction terms, which are anisotropic in the x and y directions by the parameter W , the fourth term is the biquadratic Eu-Fe exchange interaction in the form of the x -axis uniaxial anisotropy, the fifth term is the z -axis uniaxial anisotropy, and the last term is the Zeeman energy with the external field \vec{H} , which is applied in the ab plane at the angle ϕ_H with respect to the a axis. In comparison to Ref. [8], two terms, $[2Je_{1z}e_{2z}]$ and $[K_u \sum_{i=1}^2 e_{iz}^2]$, are added to complete the 3D representation of the free energy, while the Eu-Fe exchange interaction is redefined in the x -axis uniaxial form.

Following Ref. [8], exchange and anisotropy parameters of the free energy can be derived from saturation fields of the canted spin state and of the spin-flip transition as follows. When the magnetic field is applied along the b crystal axis, magnetization of Eu occurs via spin canting, and the saturation field of the spin-canted state is $H_b^{\text{sat}} = (4J + 16K_a)/M_s$. When the magnetic field is applied along the a crystal axis, magnetization saturation occurs via abrupt spin-flip transition, and the saturation field (i.e., the spin-flip field) is $H_a^{\text{sat}} = 2(J + W)/M_s$. Notice that counterintuitively H_a^{sat} and H_b^{sat} do not match each other even in the isotropic case of $W = 0$, $K_a = 0$. This is the consequence of the spin flip as the dominating magnetization process for the corresponding magnetic orientation [8]. The condition for the spin-flip transition is $J/(8K_a + W) < 1$. When the magnetic field is applied at 45° with respect to the a or b direction, the saturation field is $H_{45}^{\text{sat}} = 4J/M_s$. By expanding the treatment to the 3D case, the saturation field of the canted spin state for the field orientation along the c axis is $H_c^{\text{sat}} = (4J + 2W + 16K_a + 2K_u)/M_s$.

The dependence of orientations of Eu magnetic moments on the magnetic field can be derived numerically by minimizing the energy in Eq. (1) with predefined anisotropy and exchange parameters. By knowing the orientations of the Eu magnetic moments, the magnetic resonances of Eu can be derived using the Suhl-Smit-Beljers approach [39,40] extended for the case of magnetization dynamics in coupled magnetic multilayers [31,41–43]. With this approach the following set of equations of motion for the magnetization vector in each Eu layer defines the collective dispersion of the spin system with orientation along the ab planes ($\theta_i = \pi/2$):

$$i \frac{\omega M_s}{\gamma} \begin{bmatrix} \delta\theta_1 \\ \delta\theta_2 \\ \delta\phi_1 \\ \delta\phi_2 \end{bmatrix} = \begin{bmatrix} 0 & 0 & F_{\phi_1\phi_1} & F_{\phi_1\phi_2} \\ 0 & 0 & F_{\phi_1\phi_2} & F_{\phi_2\phi_2} \\ -F_{\theta_1\theta_1} & -F_{\theta_1\theta_2} & 0 & 0 \\ -F_{\theta_1\theta_2} & -F_{\theta_2\theta_2} & 0 & 0 \end{bmatrix} \begin{bmatrix} \delta\theta_1 \\ \delta\theta_2 \\ \delta\phi_1 \\ \delta\phi_2 \end{bmatrix}, \quad (2)$$

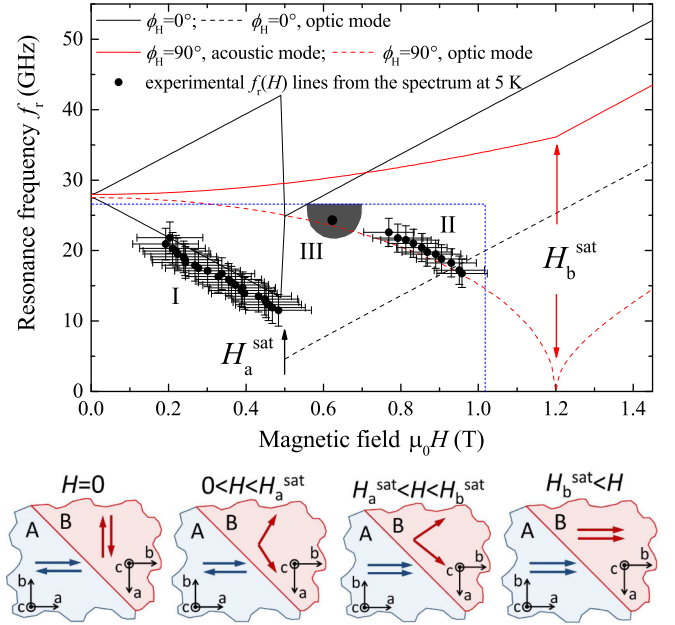


FIG. 3. Experimental and theoretical dependencies of the magnetic resonance frequency on the magnetic field $f_r(H)$. Black lines show theoretical data for the A domain with $\phi_H = 0$. Red lines show theoretical data for the B domain with $\phi_H = \pi/2$. Solid lines show either individual resonances of Eu sublattices, as in the case of $\phi_H = 0$ and $\mu_0 H < 0.5$, or the collective acoustic response. Dashed lines show the collective optical response. Arrows indicate transition fields H_a^{sat} and H_b^{sat} . Solid black circles show experimental $f_r(H)$ lines derived from the spectrum at 5 K. Error bars indicate the linewidth of experimental resonance lines $\Delta H \approx 0.17$ T and $\Delta f \approx 4.5$ GHz for line I and $\Delta H \approx 0.13$ T and $\Delta f \approx 4$ GHz for line II. The blue short-dashed line indicates the accessible range of the experimental setup. The pictograms at bottom illustrate spin configurations in twinned domains at different fields. A domains (shown in blue) correspond to domains with the spin density wave axis (a axis) aligned with the magnetic field. B domains (shown in red) correspond to domains with the spin density wave axis (a axis) aligned perpendicular to the magnetic field.

where $\delta\theta_i$ and $\delta\phi_i$ are components of small deviations of the magnetization vector in spherical coordinates, $F_{\theta_i\theta_j}$ and $F_{\phi_i\phi_j}$ are corresponding second-order partial derivatives of the free energy [Eq. (1)], ω is the eigenfrequency of magnetization precession, and $\gamma = 28$ GHz/T is the gyromagnetic ratio. Diagonal terms $F_{\theta_i\phi_j} = 0$ in Eq. (2) due to the in-plane configuration of magnetization ($\theta_i = \pi/2$). The expression $\sum \cos(\phi_i - \phi_H) \delta\phi_i$ corresponds to the dynamic susceptibility of the resonance.

Figure 3 collects experimental and theoretical dependencies of MR frequencies on the magnetic field $f_r(H)$. In calculations we consider the in-plane magnetic field aligned with the ab crystal planes, with the angle ϕ_H relative to the a crystal axis. In accordance with the twinning domain concept [6–8], the sample also contains domains where the orientation of the magnetic field is $\pi/2 - \phi_H$ relative to the a crystal axis.

In general, optimization of resonance lines with Eqs. (1) and (2) showed that the value ϕ_H is close to 0, which indicates that the sample consists of domains whose a axis is aligned

with the magnetic field and domains whose a axis is perpendicular to the magnetic field (A and B domains, respectively; see illustrations in Fig. 3). For A domains at $H < H_a^{\text{sat}}$ the spectrum consists of two antiferromagnetic spectral lines with linear-in-field increasing (decreasing) resonant frequency, attributed to individual resonances of oppositely aligned Eu spin sublattices. At $H > H_a^{\text{sat}}$ the spin-flip transition in A domains occurs, and the spectrum consists of two collective modes: the higher-frequency acoustic mode and the lower-frequency optical mode, both with linear field dependence. Antiferromagnetic interaction between layers, which are magnetized to saturation, results in higher resonance frequency for the acoustic mode in comparison to the optical mode [28,43]. For B domains with the b axis aligned with the magnetic field the spectrum also consists of two lines. At $H < H_b^{\text{sat}}$ the spectrum of B domains contains collective modes: the higher-frequency acoustic mode with positive frequency dependence on the magnetic field and the lower-frequency optical mode with negative frequency dependence on the magnetic field. At $H > H_b^{\text{sat}}$ the spin-flip transition (saturation) occurs in B domains manifested by a kink in both curves, and both collective modes show a positive dependence of the frequency on the magnetic field.

A rough numerical optimization of magnetic parameters in Eqs. (1) and (2) yields the following range for the parameters, consistent with Ref. [8], which can be used to obtain resonance curves that are consistent with the experiment: $4J/M_s \approx 0.8\text{--}0.9$ T, $2W/M_s \approx 0.1\text{--}0.2$ T, $H_a^{\text{sat}} \approx 0.45\text{--}0.55$ T, $H_b^{\text{sat}} = (4J + 16K_a)/M_s \approx 1.15\text{--}1.25$ T, $2K_u/M_s \approx 0.2\text{--}0.3$ T, and $|\phi_H| < 5^\circ$. The large width of resonance lines and limited experiential range did not allow us to perform a more accurate optimization of the parameters. Solid and dashed lines in Fig. 3 show $f_r(H)$ obtained using Eqs. (1) and (2) and the following set of parameters: $4J/M_s = 0.8$ T, $2W/M_s = 0.1$ T, $H_a^{\text{sat}} = 0.5$ T, $H_b^{\text{sat}} = (4J + 16K_a)/M_s = 1.2$ T, $2K_u/M_s = 0.25$ T, and $\phi_H = 0$. According to Fig. 3, spectral line I corresponds to the resonance of Eu spins aligned against the external field in the domain having the angle $\phi_H = 0$ with the external field. Spectral line II corresponds to the optical antiferromagnetic response in the domain having the angle $\phi_H = \pi/2$ with the external field. Its optical origin explains the low intensity in comparison to line I. The dependence of the resonance lines on the angle ϕ_H can be found in Ref. [35].

It is important to note that the presence of line I at low fields, which is the signature of the A domain, means that the mid-field detwinning stage when the B-domain population consumes the A-domain population at $\mu_0 H \sim 0.3$ T [6,7,25] does not take place. On the other side, the presence of line II at high fields up to 0.95 T, which is the signature of the B domain, means that the high-field detwinning stage when the A-domain population consumes the B-domain population at $\mu_0 H \gtrsim 0.7$ T [6,7,25] also does not take place. Therefore the experimental spectral lines in Fig. 3 evidence to some extent that the detwinning process does not take place in our EuFe_2As_2 single-crystal sample. However, the large resonance linewidth and insufficient signal-to-noise ratio do not allow us to undertake any quantitative analysis of the domain populations.

Spectral feature III in Figs. 2(a) and 3 may be attributed to the optical antiferromagnetic response in the same B do-

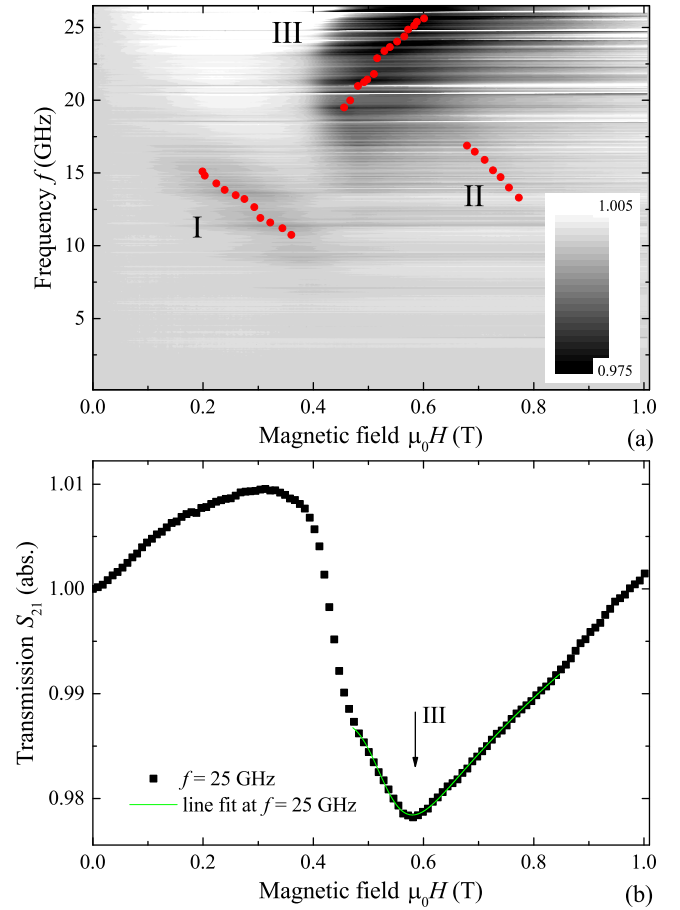


FIG. 4. (a) MR absorption spectra $S_{21}(f, H)$ of EuFe_2As_2 measured at $T = 13$ K. The magnetic field is applied in plane along the ab crystal planes. Solid red circles show the experimental resonance curves $f_r(H)$ obtained by fitting spectral lines. (b) Cross section $S_{21}(H)$ of the spectrum at $T = 13$ K at $f = 25$ GHz. The solid line in (b) shows the fit of the resonant feature.

main. In this case the change in the line intensity is the signature of the twin domain wall relocation when the fraction of these domains is reduced with the magnetic field. Alternatively, spectral feature III may be a trace of the acoustic mode of the A domain with $\phi_H = 0$ and $H > H_a^{\text{sat}}$. The origin of spectral feature III can be established by studying the temperature dependence of the spectrum. Upon increasing the measurement temperature, all spectral lines shift to lower frequencies, while the transition fields decrease [35]. Figure 4(a) shows the MR absorption spectrum of a EuFe_2As_2 sample measured with the magnetic field applied in plane along the ab layers at $T = 13$ K. The spectrum contains the same three absorption features [experimental $f_r(H)$ dependencies are shown with solid red circles]. Resonance line I at $0.2 < \mu_0 H \lesssim 0.4$ T and $10 < f < 15$ GHz corresponds to the resonance of Eu spins aligned against the external field in the A domain having the angle $\phi_H = 0$ with the external field (see schematic images in Fig. 3). A weak resonance line II at $0.7 \lesssim \mu_0 H \lesssim 0.8$ T and $12 < f < 18$ GHz corresponds to the optical antiferromagnetic response in the B domain having the angle $\phi_H = \pi/2$ with the external field. Spectral feature III at $T = 5$ K [Fig. 2(a)] is transformed at $T = 13$ K into a

clearly distinguishable resonance line at $0.45 \lesssim \mu_0 H \lesssim 0.7$ T and $18 < f < 26$ GHz with positive-slope linear dependence $f_r(H)$, thus manifesting the acoustic mode of A domains with $\phi_H = 0$ and $H > H_a^{\text{sat}}$. Lines I and III indicate that the spin-flip field at $T = 13$ K is reduced to $H_a^{\text{sat}} \approx 0.4$ T as compared with $H_a^{\text{sat}} \approx 0.5$ T at 5 K. Figure 4(b) shows the cross section of the spectrum $S_{21}(H)$ at $f = 25$ GHz. The cross section indicates a drop in the transmission at $\mu_0 H \approx 0.4$ T. This drop is attributed to the spin-flip transition of A domains but is not related to a spin resonance process. At $\mu_0 H > 0.4$ T the magnetization of the A domains is changed in a stepwise manner, which results in corresponding changes in the impedance of the transmission line and, consequently, in its transmission characteristics regardless of the resonance process. In addition, the curve $S_{21}(H)$ shows a resonance peak III at $\mu_0 H \approx 0.58$ T. The fit of the resonance peaks with the complex susceptibility allowed us to derive the resonance line $f_r(H)$, which is shown in Fig. 4(a) with solid red circles.

The overall correspondence between experimental and theoretical lines in Fig. 3 and the established nature of all lines in Figs. 3 and 4 confirm the validity of the free-energy relation in Eq. (1) with the anisotropic Eu-Eu exchange interaction and biquadratic Eu-Fe exchange interaction for the EuFe_2As_2 compound together with the domain twinning concept of its orthorhombic crystal structure.

It should be noticed that, in general, according to the temperature dependence of the spectrum [35] at higher temperatures the acoustic mode of the B domains is expected to appear in the accessible frequency range at low fields $H < H_a^{\text{sat}}$. However, the amplitude of the acoustic mode of B domains is proportional to the magnetization of B domains and thus is expected to be zero at zero fields and to show a linear increase with the magnetic field. Therefore the intensity of the acoustic mode of B domains at $H < H_a^{\text{sat}}$ is expected to be low. In addition, the low overall ferromagnetic resonance (FMR) signals [see Fig. 2(b)], large linewidth of resonance lines, proximity of this mode to line III, and abrupt change in the impedance at $H \sim H_a^{\text{sat}}$ [see Fig. 4(b)] make the acoustic mode of B domains at $H < H_a^{\text{sat}}$ unobservable. Also, according to Fig. 3, the optic mode of A domains is expected at $H > H_a^{\text{sat}}$ in the frequency range 5–20 GHz. This line is not observed experimentally in Fig. 2 due to zero dynamic susceptibility of optic modes in the uniform ac magnetic field, which is perpendicular to the magnetization direction. However, in general, in FMR experiments, optic modes appear in the spectrum if the ac field is not uniform across the thickness of the sample, if the sample itself is inhomogeneous across its thickness (inhomogeneity in exchange, anisotropy, or magnetization of the magnetic layers), or if the sample is misoriented with respect to the external field. In this regard, observation of the optic mode of the B domains [line II in Figs. 2(a) and 4(a)] indicates possible misalignment of the b axis with respect to the direction of the magnetic field, or some inhomogeneity in the B domains across the thickness of the sample. Apparently, some of these factors did not work out for the optic mode of the A domains at $H > H_a^{\text{sat}}$.

Once the validity of the Hamiltonian (1) and the origin of all three lines are established it is instructive to consider resonance properties of EuFe_2As_2 theoretically in more detail. First, it can be noticed that at zero field in Fig. 3,

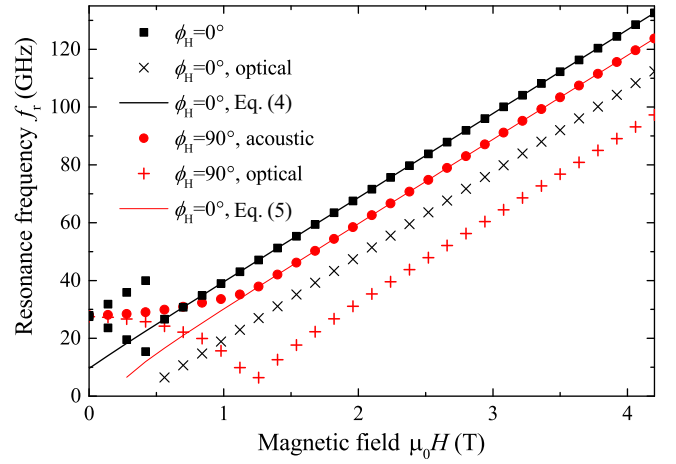


FIG. 5. Theoretical dependencies of the magnetic resonance frequency on the magnetic field $f_r(H)$ obtained numerically with Eqs. (1) and (2) using the same parameters as in Fig. 3 (symbols) and analytically with Eqs. (4) and (5) (solid lines).

resonance lines are split by $\Delta f_r \approx 0.5$ GHz. In general, for two-sublattice antiferromagnets the zero-field split occurs due to the two-axis anisotropy. From Eq. (2) at $H = 0$ it can be derived that the split in MR frequency is set by the difference between two eigenfrequencies given by the expressions

$$\left(\frac{2\pi f_r}{\mu_0\gamma}\right)^2 = (2W + 16K_a + 2K_u)(4J + 16K_a),$$

$$\left(\frac{2\pi f_r}{\mu_0\gamma}\right)^2 = (4J + 2W + 16K_a + 2K_u)(4W + 16K_a). \quad (3)$$

As follows from Eq. (3), in the case of EuFe_2As_2 the width of the split Δf_r is also affected by the anisotropy in the exchange interaction. In the isotropic case, $W = 0$ and $K_u = 0$, both expressions relax to the known textbook splitless expression [28,30]. However, it should be noticed that Δf_r is by far smaller than the linewidth of the resonance lines and thus cannot be verified directly for EuFe_2As_2 .

Next, we consider the resonance of magnetically saturated A and B domains. In terms of Eq. (1), by setting $\vec{e}_1 = \vec{e}_2$ the Suhl-Smit-Beljers approach yields for a single magnetic layer

$$\left(\frac{2\pi f_r}{\mu_0\gamma}\right)^2 = (H + 16K_a - 4W)(H + 16K_a - 2W + 2K_u) \quad (4)$$

for the higher-frequency acoustic mode of the A domain at $H > H_a^{\text{sat}}$ and

$$\left(\frac{2\pi f_r}{\mu_0\gamma}\right)^2 = (H - 16K_a + 4W)(H + 2W + 2K_u) \quad (5)$$

for the higher-frequency acoustic mode of the B domain at $H > H_b^{\text{sat}}$. Figure 5 shows theoretical dependencies of the magnetic resonance frequency on the magnetic field $f_r(H)$ obtained numerically with Eqs. (1) and (2) using the same parameters as in Fig. 3 and analytically with Eqs. (4) and (5). The consistency between corresponding resonance lines confirms the validity of the numerical studies. Interestingly, the exchange anisotropy parameter W enters into both

expressions, which can be used additionally in MR determination of magnetic properties of complex antiferromagnets. In the case in which a complete high-field detwinning of the single crystal takes place, the resonance lines $f_r(H)$ of the B domains having $\phi_H = 90^\circ$ in Fig. 5 should disappear, while the $f_r(H)$ of the A domains having $\phi_H = 0$ should remain.

IV. CONCLUSION

In conclusion, in this paper we report the results of magnetic resonance spectroscopy of EuFe_2As_2 single crystals. The spectrum reveals several resonant features attributed to antiferromagnetic resonances of the Eu sublattice. By employing the recently proposed spin Hamiltonian with anisotropic Eu-Eu exchange interaction and biquadratic Eu-Fe exchange interaction, the spectral features have been identified and attributed to antiferromagnetic and collective resonances of

Eu layers in the orthorhombic twinned crystal with different orientations of twin domains with respect to the external field. The obtained magnetic parameters are quantitatively consistent with those reported previously, thus confirming the complex biquadratic Hamiltonian for Eu spins in EuFe_2As_2 proposed earlier.

ACKNOWLEDGMENTS

The authors acknowledge the Russian Science Foundation (project N 18-72-10118) for support in experiments and the Ministry of Science and Higher Education of the Russian Federation (project N 0718-2020-0025) for support in sample characterization and theory. Crystal synthesis was done using equipment from the LPI Shared Facility Center and was partially supported by the Russian Science Foundation (project N 21-12-00394).

-
- [1] Z. Ren, Z. Zhu, S. Jiang, X. Xu, Q. Tao, C. Wang, C. Feng, G. Cao, and Z. Xu, *Phys. Rev. B* **78**, 052501 (2008).
- [2] H. S. Jeevan, Z. Hossain, D. Kasinathan, H. Rosner, C. Geibel, and P. Gegenwart, *Phys. Rev. B* **78**, 052502 (2008).
- [3] S. Jiang, Y. Luo, Z. Ren, Z. Zhu, C. Wang, X. Xu, Q. Tao, G. Cao, and Z. Xu, *New J. Phys.* **11**, 025007 (2009).
- [4] Y. Xiao, Y. Su, M. Meven, R. Mittal, C. M. N. Kumar, T. Chatterji, S. Price, J. Persson, N. Kumar, S. K. Dhar, A. Thamizhavel, and T. Brueckel, *Phys. Rev. B* **80**, 174424 (2009).
- [5] Y. Xiao, Y. Su, W. Schmidt, K. Schmalzl, C. M. N. Kumar, S. Price, T. Chatterji, R. Mittal, L. J. Chang, S. Nandi, N. Kumar, S. K. Dhar, A. Thamizhavel, and T. Brueckel, *Phys. Rev. B* **81**, 220406(R) (2010).
- [6] S. Zapf, C. Stingl, K. W. Post, J. Maiwald, N. Bach, I. Pietsch, D. Neubauer, A. Löhle, C. Clauss, S. Jiang, H. S. Jeevan, D. N. Basov, P. Gegenwart, and M. Dressel, *Phys. Rev. Lett.* **113**, 227001 (2014).
- [7] J. Maiwald, I. I. Mazin, and P. Gegenwart, *Phys. Rev. X* **8**, 011011 (2018).
- [8] J. J. Sanchez, G. Fabbris, Y. Choi, Y. Shi, P. Malinowski, S. Pandey, J. Liu, I. I. Mazin, J.-W. Kim, P. Ryan, and J. H. Chu, *Phys. Rev. B* **104**, 104413 (2021).
- [9] Z. Ren, Q. Tao, S. Jiang, C. Feng, C. Wang, J. Dai, G. Cao, and Z. Xu, *Phys. Rev. Lett.* **102**, 137002 (2009).
- [10] G. Cao, S. Xu, Z. Ren, S. Jiang, C. Feng, and Z. Xu, *J. Phys.: Condens. Matter* **23**, 464204 (2011).
- [11] H. S. Jeevan, D. Kasinathan, H. Rosner, and P. Gegenwart, *Phys. Rev. B* **83**, 054511 (2011).
- [12] S. Nandi, W. T. Jin, Y. Xiao, Y. Su, S. Price, D. K. Shukla, J. Stremper, H. S. Jeevan, P. Gegenwart, and T. Brueckel, *Phys. Rev. B* **89**, 014512 (2014).
- [13] V. S. Stolyarov, I. S. Veshchunov, S. Y. Grebenchuk, D. S. Baranov, I. A. Golovchanskiy, A. G. Shishkin, N. Zhou, Z. Shi, X. Xu, S. Pyon, Y. Sun, W. Jiao, G.-H. Cao, L. Ya. Vinnikov, A. A. Golubov, T. Tamegai, A. I. Buzdin, and D. Roditchev, *Sci. Adv.* **4**, eaat1061 (2018).
- [14] S. Y. Grebenchuk, Z. A. Devizorova, I. A. Golovchanskiy, I. V. Shchetinin, G.-H. Cao, A. I. Buzdin, D. Roditchev, and V. S. Stolyarov, *Phys. Rev. B* **102**, 144501 (2020).
- [15] Y. Liu, Y.-B. Liu, Z.-T. Tang, H. Jiang, Z.-C. Wang, A. Ablimit, W.-H. Jiao, Q. Tao, C.-M. Feng, Z.-A. Xu, and G. H. Cao, *Phys. Rev. B* **93**, 214503 (2016).
- [16] Y. Liu, Y.-B. Liu, Y.-L. Yu, Q. Tao, C.-M. Feng, and G.-H. Cao, *Phys. Rev. B* **96**, 224510 (2017).
- [17] P. M. Smylie, K. Willa, J.-K. Bao, K. Ryan, Z. Islam, H. Claus, Y. Simsek, Z. Diao, A. Rydh, A. E. Koshelev, W.-K. Kwok, D. Y. Chung, M. G. Kanatzidis, and U. Welp, *Phys. Rev. B* **98**, 104503 (2018).
- [18] T. K. Kim, K. S. Pervakov, D. V. Evtushinsky, S. W. Jung, G. Poelchen, K. Kummer, V. A. Vlasenko, A. V. Sadakov, A. S. Usoltsev, V. M. Pudalov, D. Roditchev, V. S. Stolyarov, D. V. Vyalikh, V. Borisov, R. Valenti, A. Ernst, S. V. Ereemeev, and E. V. Chulkov, *Phys. Rev. B* **103**, 174517 (2021).
- [19] T. K. Kim, K. S. Pervakov, V. A. Vlasenko, A. V. Sadakov, A. S. Usoltsev, D. V. Evtushinsky, S. Jung, G. Poelchen, K. Kummer, D. Roditchev, V. S. Stolyarov, I. A. Golovchanskiy, D. V. Vyalikh, V. Borisov, R. Valenti, A. Ernst, S. V. Ereemeev, E. V. Chulkov, and V. M. Pudalov, *Phys. Usp.* **65** (2022), doi: 10.3367/UFNe.2021.05.039018.
- [20] K. Iida, Y. Nagai, S. Ishida, M. Ishikado, N. Murai, A. D. Christianson, H. Yoshida, Y. Inamura, H. Nakamura, A. Nakao, K. Munakata, D. Kagerbauer, M. Eisterer, K. Kawashima, Y. Yoshida, H. Eisaki, and A. Iyo, *Phys. Rev. B* **100**, 014506 (2019).
- [21] S. Ishida, D. Kagerbauer, S. Holleis, K. Iida, K. Munakata, A. Nakao, A. Iyo, H. Ogino, K. Kawashima, M. Eisterer, and H. Eisaki, *Proc. Natl. Acad. Sci. USA* **118**, e2101101118 (2021).
- [22] T. Terashima, M. Kimata, H. Satsukawa, A. Harada, K. Hazama, S. Uji, H. S. Suzuki, T. Matsumoto, and K. Murata, *J. Phys. Soc. Jpn.* **78**, 083701 (2009).
- [23] N. Kurita, M. Kimata, K. Kodama, A. Harada, M. Tomita, H. S. Suzuki, T. Matsumoto, K. Murata, S. Uji, and T. Terashima, *Phys. Rev. B* **88**, 224510 (2013).
- [24] J. Herrero-Martin, V. Scagnoli, C. Mazzoli, Y. Su, R. Mittal, Y. Xiao, T. Brueckel, N. Kumar, S. K. Dhar, A. Thamizhavel, and L. Paolasini, *Phys. Rev. B* **80**, 134411 (2009).
- [25] Q.-P. Ding, N. S. Sangeetha, W. R. Meier, M. Xu, S. L. Bud'ko, P. C. Canfield, D. C. Johnston, and Y. Furukawa, *Phys. Rev. B* **102**, 180406(R) (2020).

- [26] Z. Xu, J. Pan, Z. Tao, R. Liu, and G. Tan, *Chin. Phys. B* **29**, 077402 (2020).
- [27] T. Nagamiya, K. Yosida, and R. Kubo, *Adv. Phys.* **4**, 1 (1955).
- [28] *Magnetization Oscillations and Waves*, edited by A. G. Gurevich and G. A. Melkov (CRC, Boca Raton, FL, 1996).
- [29] A. N. Bogdanov, A. V. Zhuravlev, and U. K. Röbber, *Phys. Rev. B* **75**, 094425 (2007).
- [30] S. M. Rezende, A. Azevedo, and R. L. Rodríguez-Suárez, *J. Appl. Phys. (Melville, NY)* **126**, 151101 (2019).
- [31] I. Golovchanskiy and V. Stolyarov, *J. Appl. Phys. (Melville, NY)* **131**, 053901 (2022).
- [32] I. A. Golovchanskiy, E. I. Maltsev, I. V. Shchetinin, V. A. Vlasenko, P. S. Dzhumaev, K. Pervakov, O. V. Emelyanova, A. Y. Tsvetkov, N. N. Abramov, V. M. Pudalov, and V. S. Stolyarov, [arXiv:2204.00389](https://arxiv.org/abs/2204.00389).
- [33] K. S. Pervakov, V. A. Vlasenko, E. P. Khlybov, A. Zaleski, V. M. Pudalov, and Y. F. Eltsev, *Supercond. Sci. Technol.* **26**, 015008 (2013).
- [34] V. Vlasenko, K. Pervakov, and S. Gavrilkin, *Supercond. Sci. Technol.* **33**, 084009 (2020).
- [35] See Supplemental Material at <http://link.aps.org/supplemental/10.1103/PhysRevB.106.024412> for results of FMR spectroscopy at different temperatures, for test magnetization measurements, and for theoretical plots of spectral lines at different orientations with respect to the external field.
- [36] I. Neudecker, G. Woltersdorf, B. Heinrich, T. Okuno, G. Gubbiotti, and C. H. Back, *J. Magn. Magn. Mater.* **307**, 148 (2006).
- [37] S. S. Kalarickal, P. Krivosik, M. Wu, C. E. Patton, M. L. Schneider, P. Kabos, T. J. Silva, and J. P. Nibarger, *J. Appl. Phys. (Melville, NY)* **99**, 093909 (2006).
- [38] D. MacNeill, J. T. Hou, D. R. Klein, P. Zhang, P. Jarillo-Herrero, and L. Liu, *Phys. Rev. Lett.* **123**, 047204 (2019).
- [39] H. Suhl, *Phys. Rev.* **97**, 555 (1955).
- [40] J. Smit and H. G. Beljers, *Philips Res. Rep.* **10**, 113 (1955).
- [41] Z. Zhang, L. Zhou, P. E. Wigen, and K. Ounadjela, *Phys. Rev. B* **50**, 6094 (1994).
- [42] D. S. Schmooly and J. M. Barandiaran, *J. Phys.: Condens. Matter* **10**, 10679 (1998).
- [43] J. Lindner and K. Baberschke, *J. Phys.: Condens. Matter* **15**, S465 (2003).